JACS
JOURNAL OF THE AMERICAN CHEMICAL SOCIETY
pubs.acs.org/JACS
Communication

A New Class of Molecular Electrocatalysts for Hydrogen Evolution: Catalytic Activity of $M_3N@C_{2n}$ ($2n$ = 68, 78, and 80) Fullerenes

Alain R. Puente Santiago,* Mohamed Fathi Sanad, Antonio Moreno-Vicente, Md Ariful Ahsan, Maira R. Cerón, Yang-Rong Yao, Sreeprasad T. Sreenivasan, Antonio Rodriguez-Fortea, Josep M. Poblet,* and Luis Echegoyen*

Cite This: J. Am. Chem. Soc. 2021, 143, 6037−6042

ABSTRACT: The electrocatalytic properties of some endohedral fullerenes for hydrogen evolution reactions (HER) were recently predicted by DFT calculations. Nonetheless, the experimental catalytic performance under realistic electrochemical environments of these 0D-nanomaterials have not been explored. Here, for the first time, we disclose the HER electrocatalytic behavior of seven $M_3N@2n$ ($2n$ = 68, 78, and 80) fullerenes ($Gd_3N@I_h(7)$-C_{80}, $Y_3N@I_h(7)$-C_{80}, $Lu_3N@I_h(7)$-C_{80}, $Sc_3N@I_h(7)$-C_{80}, $Sc_3N@D_{5h}(6)$-C_{80}, $Sc_3N@D_{3h}(5)$-C_{78}, and $Sc_3N@D_3(6140)$-C_{68}) using a combination of experimental and theoretical techniques. The non-IPR $Sc_3N@D_3(6140)$-C_{68} compound exhibited the best catalytic performance toward the generation of molecular hydrogen, exhibiting an onset potential of −38 mV vs RHE, a very high mass activity of 1.75 A·mg^{-1} at −0.4 V vs RHE, and an excellent electrochemical stability, retaining 96% of the initial current after 24 h. The superior performance was explained on the basis of the fused pentagon rings, which represent a new and promising HER catalytic motif.

Low-dimensional (LD) carbon-based nanomaterials have recently sparked increasing interest as efficient catalysts for proton electroreduction processes due to their remarkable electronic properties, low costs, large surface areas, variable molecular structures, and excellent tolerances to acid/alkaline media.[1−5] Among the most successful HER carbon-based LD catalysts are graphene,[6] onion-like graphene structures,[7] carbon nanotubes,[8] graphitic carbon nitride,[9] and boron carbon nitride nanosheets.[10] Although these LD platforms efficiently catalyze electrochemical proton reduction reactions, their intrinsic activities are lower than those of their metal-based counterparts.[11]

Several strategies have been attempted to maximize the intrinsic HER catalytic activity of LD carbon-based nanomaterials.[12−16] The overall electrocatalytic yields are mainly controlled by the adsorption energy of the reaction intermediates and the electronic properties of the catalyst surfaces.[17] Therefore, the introduction of single metal atoms into the sp^2 carbon framework has been explored to engineer the electronic structure and increase the catalytic performance of the materials.[18] It has been discovered that Pt atom sites deposited onto the curved structures of carbon nano-onions promote highly active local electric fields, thus greatly improving the reaction kinetics for hydrogen evolution.[18] This suggests that the interaction of single metallic atoms with sp^2 curved carbon networks substantially decreases the energy adsorption states of the intermediate catalytic species for HER electrocatalysis. Endohedral fullerenes, which typically contain metal species in hollow fullerene cavities, have been theoretically described as unique LD HER catalysts.[19]

Aijun and co-workers theoretically predicted that when a metal is trapped inside C_{60} the surface carbon atoms become catalytically active as a consequence of a variation of their electronic density of states due to the effective electron transfer from the encapsulated metal to the cage, as opposed to metal-based LD materials.[20] To the best of our knowledge, the HER catalytic properties of endohedral fullerenes have not been experimentally investigated to date.

In this work, the electrocatalytic HER properties of seven endohedral fullerenes ($Gd_3N@I_h(7)$-C_{80}, $Y_3N@I_h(7)$-C_{80}, $Lu_3N@I_h(7)$-C_{80}, $Sc_3N@I_h(7)$-C_{80}, $Sc_3N@D_{5h}(6)$-C_{80}, $Sc_3N@D_{3h}(5)$-C_{78}, and $Sc_3N@D_3(6140)$-C_{68}) have been experimentally and theoretically investigated. The role of the metal, symmetry, number of carbon atoms, and non-IPR sites on the catalytic performance were explored. The main hypothesis driving this work was that the presence of [5,5] or fused pentagon rings (pentalenes units) should perform as reasonably active catalytic sites for H^+ attachment and for the consequent formation of hydrogen. Impressively, $Sc_3N@D_3(6140)$-C_{68} significantly outperformed the catalytic activity of all of the endohedral metallofurenes (EMF) studied here, exhibiting an impressive onset potential value of −38 mV vs RHE and a very remarkable mass activity of 1.75 A·mg^{-1} at −0.4 V vs RHE. This outstanding catalytic performance was ascribed to the three pentalene sites. Theoretical calculations and experimental results indicate that the highest negative charge density on non-isolated pentagon rule (non-IPR) EMFs

Received: December 15, 2020
Published: April 6, 2021

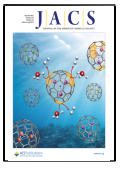

https://doi.org/10.1021/jacs.0c13002
J. Am. Chem. Soc. 2021, 143, 6037−6042

is concentrated on the pentalenes.[21] This is the first time, to the best of our knowledge, that the structure/catalytic function relationship of EMFs has been explored using a combination of experimental and theoretical techniques.

Figure 1 displays the ball-and-stick structures of three of the EMFs studied in this work. Their X-ray crystallographic structures have been reported (see the Supporting Information for more details). Although the electronic structures of $M_3N@C_{2n}$ EMFs can be rationalized using the ionic model $(M_3N)^{6+}(C_{2n})^{6-}$,[22] which states that there is a formal transfer of $6e^-$ from the internal cluster to the fullerene, very well-defined structural differences can be distinguished. For instance, while Sc_3N adopts a perfectly planar structure inside C_{80}, Gd_3N, Lu_3N, and Y_3N show pyramidalized configurations (Figure S1). Most importantly, the non-IPR $Sc_3N@D_3(6140)$-C_{68} compound exhibits very peculiar structural features. $Sc_3N@D_3(6140)$-C_{68} clearly exhibits interactions between the Sc ions and the three negatively charged pentalene units that stabilize the electronic structure of the compound (Figure 1c,d).

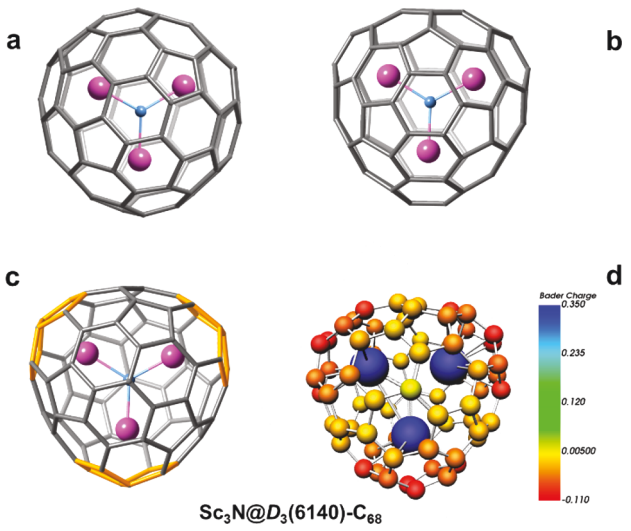

Figure 1. Ball-and-stick representation for (a) $Sc_3N@I_h(7)$-C_{80}, (b) $Sc_3N@D_{3h}(5)$-C_{78}, and (c) $Sc_3N@D_3(6140)$-C_{68}. (d) Computed atomic charges for $Sc_3N@D_3(6140)$-C_{68}.

The proton electroreduction properties of the metallofullerenes were explored using linear sweep voltammetry (LSV) in 0.5 M H_2SO_4. Figure 2 shows the catalytic activity of the EMFs for hydrogen evolution. Both the onset potential and the current densities of the seven compounds amply surpass the values measured for the empty fullerenes (C_{60} and C_{70}), indicating that the effective electron transfer from the metal clusters to the cages influence the hydrogen adsorption energy values, in agreement with a recent theoretical report.[20] The HER catalytic activities of $Sc_3N@I_h(7)$-C_{80}, $Sc_3N@D_{3h}(5)$-C_{78}, $Sc_3N@D_{5h}(6)$-C_{80}, $Gd_3N@I_h(7)$-C_{80}, $Y_3N@I_h(7)$-C_{80}, and $Lu_3N@I_h(7)$-C_{80} are similar, indicating that their structural variations, based mainly on the nature of the metal, symmetries, and degree of pyramidalization of the metal clusters do not play a significant role in their catalytic performances. Interestingly, $Sc_3N@D_3(6140)$-C_{68} decisively

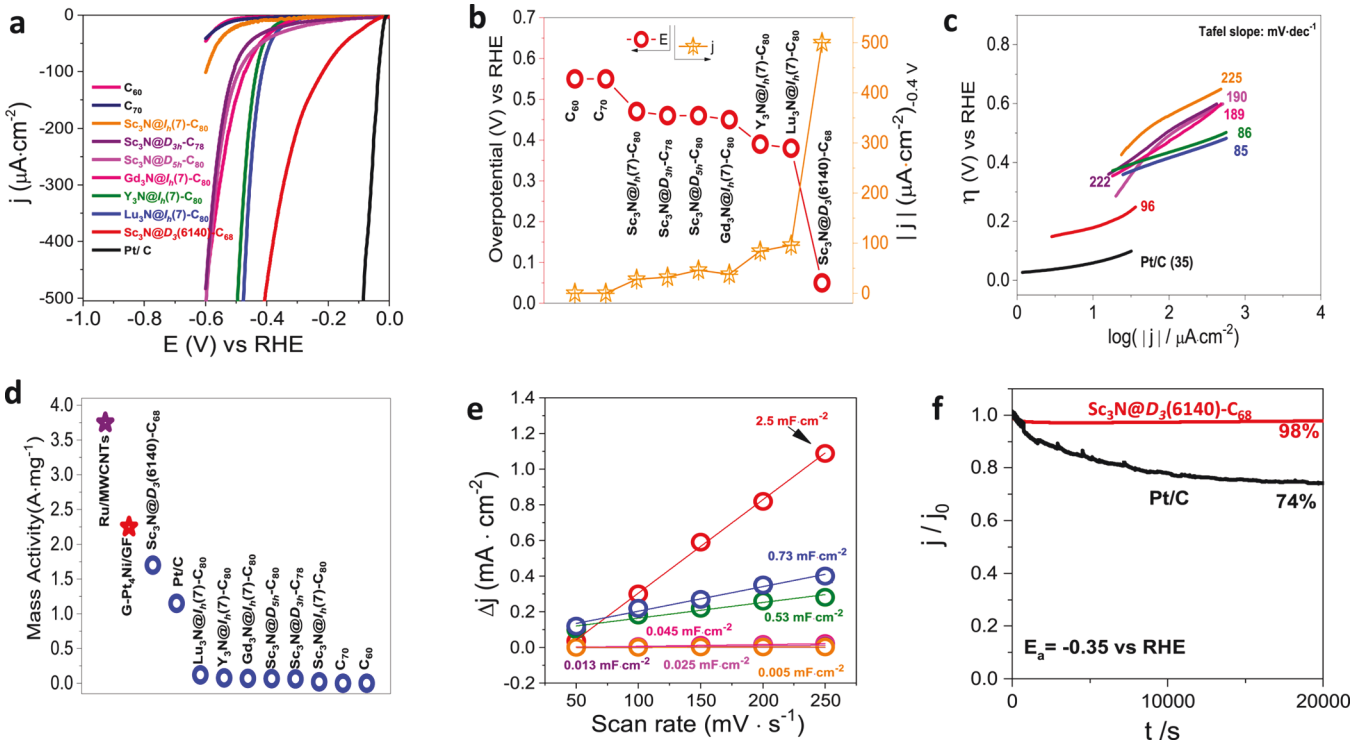

Figure 2. (a) LSVs of HER for C_{60}, C_{70}, $Gd_3N@I_h(7)$-C_{80}, $Y_3N@I_h(7)$-C_{80}, $Lu_3N@I_h(7)$-C_{80}, $Sc_3N@I_h(7)$-C_{80}, $Sc_3N@D_{5h}(6)$-C_{80}, $Sc_3N@D_{3h}(5)$-C_{78}, and $Sc_3N@D_3(6140)$-C_{68} and Pt/C at 2 $mV{\cdot}s^{-1}$ in 0.5 M H_2SO_4. (b) Onset overpotential and current density HER values for C_{60}, C_{70}, $Gd_3N@I_h(7)$-C_{80}, $Y_3N@I_h(7)$-C_{80}, $Lu_3N@I_h(7)$-C_{80}, $Sc_3N@I_h(7)$-C_{80}, $Sc_3N@D_{5h}(6)$-C_{80}, $Sc_3N@D_{3h}(5)$-C_{78}, and $Sc_3N@D_3(6140)$-C_{68}. (c) Corresponding Tafel plots of the EMFs and Pt/C. (d) Mass activity values of EMFs, Pt/C and other state-of-the-art catalysts at −0.4 V vs RHE. (e) Δj vs scan rate for the EMF catalysts. (f) I–t curves for $Sc_3N@D_3(6140)$-C_{68} and Pt/C.

https://doi.org/10.1021/jacs.0c13002
J. Am. Chem. Soc. 2021, 143, 6037−6042

outperformed the HER activities of all the EMFs, exhibiting a very low onset potential of −38 mV vs RHE and an amplified current density of 500 $\mu A \cdot cm^{-2}$ at −0.4 V, which is ∼5 times larger when compared with the currents observed for $Gd_3N@I_h(7)$-C_{80}, $Y_3N@I_h(7)$-C_{80}, and $Lu_3N@I_h(7)$-C_{80} at the same electrochemical potential (Figure 2a,b). The ECSA-normalized LSVs of the EMFs show the higher intrinsic catalytic activity of $Sc_3N@D_3(6140)$-C_{68} (Figure S2). Additionally, the observed onset potential is comparable to those observed for state-of-the-art metal functionalized LD HER catalysts (Table S1). We propose that the enhanced catalytic activity of the $Sc_3N@D_3(6140)$-C_{68} catalyst can be understood on the basis of the relatively high negative charge densities on the pentalene groups, which can favor the adsorption of the intermediate catalytic species and significantly improve the catalytic HER rates. The Tafel plots revealed key details to understand the underlying HER mechanisms for the EMF surfaces (Figure 2c). $Gd_3N@I_h(7)$-C_{80}, $Sc_3N@I_h(7)$-C_{80}, $Sc_3N@D_{3h}(5)$-C_{78}, and $Sc_3N@D_{5h}(6)$-C_{80} display very high Tafel slope values between 189 and 225 $mV \cdot s^{-1}$, indicating that the Volmer step is mainly controlling the catalytic processes, thus leading to sluggish kinetics on the fullerene surfaces. Notably, the behavior is completely different for $Sc_3N@D_3(6140)$-C_{68}, $Lu_3N@I_h(7)$-C_{80}, and $Y_3N@I_h(7)$-C_{80}. The notable decrease of the Tafel plot slopes confirmed that the electrocatalytic mechanisms follow a more efficient pathway (probably Volmer−Heyrovsky), suggesting a better HER kinetic efficiency. To further understand the intrinsic catalytic activity of the EMFs, their mass activity values at −0.4 V vs RHE were determined (Figure 2d). Remarkably, the $Sc_3N@D_3(6140)$-C_{68} catalyst delivered a superior mass activity value of 1.75 $A \cdot mg^{-1}$, which is by far better than for the other EMFs and close to other top-performing metal-containing LD nanocatalysts (Table S2). The superior intrinsic catalytic performance of the non-IPR fullerene was verified by double-layer capacitance (C_{DL}) studies (Figures 2e and S3 and the Supporting Information for the capacitance study). The capacitance value was estimated to be 2.5 $mF \cdot cm^{-2}$, which is at least three times the value estimated for $Lu_3N@I_h(7)$-C_{80} and comparable with those for metal functionalized LD HER catalysts.[23−27] These results demonstrate the higher number of accessible catalytic sites of $Sc_3N@D_3(6140)$-C_{68}, which exhibits a TOF value of 2.35 s^{-1}(see the Supporting Information for TOF calculation). Additionally, $Sc_3N@D_3(6140)$-C_{68} showed an outstanding electrochemical long-term stability in acid environments, retaining 98 and 96% of the initial current applied after 5.6 and 24 h, respectively (Figures 2f and S4). The EMF does not exhibit notable structural changes after 24 h (Figure S5). An overall water splitting device was fabricated using the $Sc_3N@D_3(6140)$-C_{68} as anode and cathode, due to its good OER properties (Figure S6).[28] It delivered a cell voltage of 1.69 V to achieve 10 $mA \cdot cm^{-2}$ (Figure S7).

Mott−Schottky (M-S) analyses were carried out to investigate the available charge carrier densities (N_d) for HER of the EMFs (Figures 3 and S8 and Supporting Information for the M-S study). It is well-known that the correlation between the M-S plots and N_d is negative, which means as slope decreases, the N_d increases, thus improving the charge carrier densities, and in turn, the electron transfer kinetics. $Sc_3N@D_3(6140)$-C_{68} exhibited the lowest slope among all the fullerene catalysts, indicating that the non-IPR

Figure 3. M-S analyses of the EMFs.

fullerene has the largest number of charge carriers, which significantly enhance the charge transfer at the M-S interfaces. Figure 3 shows M-S analyses of the endohedral catalysts. Note that the calculated Fermi level for $Sc_3N@D_3(6140)$-C_{68} is the closest value to that for the standard hydrogen evolution potential (0 eV).

To better understand the role of pentalene units in the generation of H_2 at low reduction potentials, we have performed DFT calculations. In particular, we compared the proton and electron affinities of C_{60} with those of the prototypical IPR $Sc_3N@C_{80}$ and of the non-IPR $Sc_3N@D_3(6140)$-C_{68}, using approaches employed in the analysis of redox properties of fullerenes and polyoxoanions.[29−31]

The protonation energies for $Sc_3N@D_3(6140)$-C_{68} were computed to be significantly more exergonic than for C_{60}. For instance, whereas the protonation process for C_{60} is endothermic by +0.21 eV, for $Sc_3N@C_{68}$, it is exothermic by −0.76 eV. We have observed a similar trend for the second proton (Table 1). Table 1 also includes the LUMO energy

Table 1. Comparison of LUMO Energies and Proton Adsorption Energies for Neutral and Protonated Fullerenes

	LUMO[a]			ΣE_{H^+}[b]	
	$m = 0$	$m = 1$	$m = 2$	$m = 1$	$m = 2$
$C_{60}H_m^{m+}$	−4.15	−5.28	−5.53	+0.21	−0.09
$Sc_3N@C_{68}H_m^{m+}$	−3.45	−4.20	−4.97	−0.76	−1.42
$Sc_3N@C_{80}H_m^{m+}$	−3.55	−4.27	−5.11	−0.53	−0.62

[a]LUMO energy in water for neutral, monoprotonated and diprotonated fullerenes. [b]Energies associated to process Fullerene + $mH_3O^+ \rightarrow$ Fullerene-H_m^{m+} + mH_2O.

levels for C_{60}, $Sc_3N@C_{68}H_m^{m+}$ and $Sc_3N@C_{80}H_m^{m+}$ at different protonation states. Interestingly, although $Sc_3N@D_3(6140)$-C_{68} is the fullerene with the highest LUMO, it decreases by 0.75 eV with the attachment of the first proton and by 1.52 eV when two protons are bound to the carbon surface, indicating that the protonation degree dramatically changes the redox properties of the fullerene upon proton adsorption on the pentalene units.

The free energy associated with the release of H_2 once the fullerene is reduced (i.e., the free energy (ΔG_{H_2}) associated with the $Sc_3N@C_{68}H_2 \rightarrow Sc_3N@C_{68} + H_2$ process) is exergonic by −0.20 eV. The behavior is different for $Sc_3N@C_{80}$, for which the first proton is favorably adsorbed by −0.53 eV, but the energetic gain for the adsorption of the second proton is only 0.09 eV. The release of H_2 occurs once the

https://doi.org/10.1021/jacs.0c13002
J. Am. Chem. Soc. 2021, 143, 6037−6042

fullerene is reduced (ΔG_{H_2} = −0.68 eV) and is more favorable than that for $Sc_3N@C_{68}H_2$, a result that is consistent with the high stability of the bare IPR endofullerene.[32]

These findings suggest that the applied potential to *activate* the catalysts determines the *onset potential* of the HER process. Combining experimental and theoretical observations, we propose in Figure 4 the activation mechanisms for the three catalysts studied.

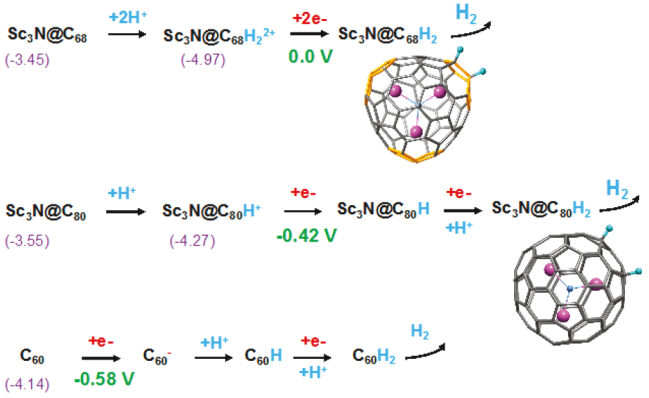

Figure 4. Schematic representation of the initial steps of HER mechanism catalyzed by C_{60}, $Sc_3N@C_{68}$ and $Sc_3N@C_{80}$. LUMO energies (in eV) are in parentheses and overpotentials relative to $Sc_3N@C_{68}$ are in V (see Scheme S1).

Notably, while for C_{60}, the fullerene is only activated after 1e-reduction because of its relatively low proton affinity, $Sc_3N@C_{80}$ and $Sc_3N@D_3(6140)$-C_{68} can be initially protonated, thus lowering their relatively high reduction potentials. In particular, $Sc_3N@D_3(6140)$-C_{68} can be easily protonated twice in acid environments, forming $Sc_3N@C_{68}H_2^{2+}$ species with a rather deep LUMO that can be reduced at very low potentials to produce the neutral $Sc_3N@C_{68}H_2$. For $Sc_3N@C_{80}$, the activation process of the catalyst is slightly different. Thus, while the monoprotonation is favorable, the adsorption of a second proton is much less so (Table 1), and given that $Sc_3N@C_{80}H^+$ can be reduced at a lower potential than the bare C_{60}, we assume that the $Sc_3N@C_{80}H^+ \rightarrow Sc_3N@C_{80}H$ step determines the onset potential for this electrocatalyst. From the 1e-reduction energies given in Scheme S1, we estimated that the *relative* overpotentials for $Sc_3N@I_h(7)$-C_{80} and C_{60} with respect to that for $Sc_3N@D_3(6140)$-C_{68} are −0.42 and −0.58 V, respectively, which are close to the experimental values. A similar trend is obtained for the Fermi levels obtained from the M-S analyses (Figure 3).

At the onset potential, the current densities quickly increase, particularly for $Sc_3N@D_3(6140)$-C_{68} (Figure 2a). This means that more carbon sites are probably activated by successive electron reductions and proton adsorptions. The rather low ΔG_{H^*} value of −0.13 eV computed for $Sc_3N@D_3(6140)$-$C_{68}H_{12}$[33,34] suggests that high degrees of hydrogenation favor the generation of H_2. The lowest energy distribution of 12H on the $Sc_3N@D_3(6140)$-C_{68} and its ΔG_{H^*} can be found in Figure S9 and Table S3, respectively.

In summary, we have determined that the non-IPR $Sc_3N@D_3(6140)$-C_{68} exhibits an impressive HER activity. This ability seems to be closely related to the pentalene motifs, which can significantly lower the LUMO energy values after proton adsorption as well as greatly facilitate the hydrogen protonation, thus increasing the overall catalytic rates. Further studies are being carried out in our laboratories to fully understand the diverse factors that control the generation of H_2 catalyzed by EMFs.

■ ASSOCIATED CONTENT

Supporting Information

The Supporting Information is available free of charge at https://pubs.acs.org/doi/10.1021/jacs.0c13002.

Synthetic details of the EMFs. Double-layer capacitance measurements. Turnover frequency number estimation. OER polarization curves of the EMFs. Catalytic performance of the overall water splitting device. Tauc and M-S plots for the EMFs. Additional computational details for the HER mechanism of the EMFs. (PDF)

■ AUTHOR INFORMATION

Corresponding Authors

Alain R. Puente Santiago − *Department of Chemistry, University of Texas at El Paso, El Paso, Texas 79968, United States;* orcid.org/0000-0002-8491-3565; Email: arpuentesan@utep.edu

Josep M. Poblet − *Departmento de Química Física i Inorgànica, Universitat Rovira i Virgili, 43007 Tarragona, Spain;* orcid.org/0000-0002-4533-0623; Email: josepmaria.poblet@urv.cat

Luis Echegoyen − *Department of Chemistry, University of Texas at El Paso, El Paso, Texas 79968, United States;* orcid.org/0000-0003-1107-9423; Email: echegoyen@utep.edu

Authors

Mohamed Fathi Sanad − *Department of Chemistry and Department of Environmental Sciences and Engineering, University of Texas at El Paso, El Paso, Texas 79968, United States*

Antonio Moreno-Vicente − *Departmento de Química Física i Inorgànica, Universitat Rovira i Virgili, 43007 Tarragona, Spain*

Md Ariful Ahsan − *Department of Chemistry, University of Texas at El Paso, El Paso, Texas 79968, United States;* orcid.org/0000-0002-2024-8690

Maira R. Cerón − *Lawrence Livermore National Laboratory, Livermore, California 94550, United States;* orcid.org/0000-0002-5151-0479

Yang-Rong Yao − *Department of Chemistry, University of Texas at El Paso, El Paso, Texas 79968, United States*

Sreeprasad T. Sreenivasan − *Department of Chemistry, University of Texas at El Paso, El Paso, Texas 79968, United States;* orcid.org/0000-0002-5728-0512

Antonio Rodriguez-Fortea − *Departmento de Química Física i Inorgànica, Universitat Rovira i Virgili, 43007 Tarragona, Spain;* orcid.org/0000-0001-5884-5629

Complete contact information is available at: https://pubs.acs.org/10.1021/jacs.0c13002

Notes

The authors declare no competing financial interest.

■ ACKNOWLEDGMENTS

L.E. thanks the NSF for the generous support of this work under CHE-1801317. The Robert A. Welch Foundation is also

gratefully acknowledged for an endowed chair to L.E. (grant AH-0033). J.M.P. and A.R.-F. thank the Spanish Ministry of Science (grant CTQ2017-87269-P), the Generalitat de Catalunya (grant 2017SGR629), and the URV for support. J.M.P. also thanks to the ICREA foundation for an ICREA ACADEMIA award.

REFERENCES

(1) Voiry, D.; Shin, H. S.; Loh, K. P.; Chhowalla, M. Low-dimensional catalysts for hydrogen evolution and CO_2 reduction. *Nat. Rev. Chem.* **2018**, *2* (1), 0105.

(2) Wang, L.; Pumera, M. Electrochemical catalysis at low dimensional carbons: Graphene, carbon nanotubes and beyond - A review. *Appl. Mater. Today* **2016**, *5*, 134−141.

(3) Jin, H. Y.; Guo, C. X.; Liu, X.; Liu, J. L.; Vasileff, A.; Jiao, Y.; Zheng, Y.; Qiao, S. Z. Emerging Two-Dimensional Nanomaterials for Electrocatalysis. *Chem. Rev.* **2018**, *118* (13), 6337−6408.

(4) Ahsan, M. A.; Puente Santiago, A. R.; Sanad, M. F; Mark Weller, J.; Fernandez-Delgado, O.; Barrera, L. A.; Maturano-Rojas, V.; Alvarado-Tenorio, B.; Chan, C. K.; Noveron, J. C. Tissue paper-derived porous carbon encapsulated transition metal nanoparticles as advanced non-precious catalysts: Carbon-shell influence on the electrocatalytic behaviour. *J. Colloid Interface Sci.* **2021**, *581*, 905−918.

(5) Gao, K.; Wang, B.; Tao, L.; Cunning, B. V.; Zhang, Z. P.; Wang, S. Y.; Ruoff, R. S.; Qu, L. T. Efficient Metal-Free Electrocatalysts from N-Doped Carbon Nanomaterials: Mono-Doping and Co-Doping. *Adv. Mater.* **2019**, *31* (13), 1805121.

(6) Huang, H. J.; Yan, M. M.; Yang, C. Z.; He, H. Y.; Jiang, Q. G.; Yang, L.; Lu, Z. Y.; Sun, Z. Q.; Xu, X. T.; Bando, Y.; Yamauchi, Y. Graphene Nanoarchitectonics: Recent Advances in Graphene-Based Electrocatalysts for Hydrogen Evolution Reaction. *Adv. Mater.* **2019**, *31* (48), 1903415.

(7) Nguyen, V. T.; Le, P. A.; Hsu, Y. C.; Wei, K. H. Plasma-Induced Exfoliation Provides Onion-Like Graphene-Surrounded MoS2 Nanosheets for a Highly Efficient Hydrogen Evolution Reaction. *ACS Appl. Mater. Interfaces* **2020**, *12* (10), 11533−11542.

(8) Gong, Y.; Wang, L. N.; Xiong, H. L.; Shao, M. F.; Xu, L. D.; Xie, A.; Zhuang, S. X.; Tang, Y.; Yang, X. J.; Chen, Y. M.; Wan, P. Y. 3D self-supported Ni nanoparticle@N-doped carbon nanotubes anchored on NiMoN pillars for the hydrogen evolution reaction with high activity and anti-oxidation ability. *J. Mater. Chem. A* **2019**, *7* (22), 13671−13678.

(9) Gao, M.; Liu, D. N.; Yang, H. H.; Huang, H.; Luo, Q.; Huang, Y. F.; Yu, X. F.; Chu, P. K. Modification of Layered Graphitic Carbon Nitride by Nitrogen Plasma for Improved Electrocatalytic Hydrogen Evolution. *Nanomaterials* **2019**, *9* (4), 568.

(10) Song, F. Z.; Li, W.; Yang, J. Q.; Han, G. Q.; Yan, T.; Liu, X.; Rao, Y.; Liao, P. L.; Cao, Z.; Sun, Y. J. Interfacial Sites between Cobalt Nitride and Cobalt Act as Bifunctional Catalysts for Hydrogen Electrochemistry. *ACS Energy Lett.* **2019**, *4* (7), 1594−1601.

(11) Wang, X. S.; Vasileff, A.; Jiao, Y.; Zheng, Y.; Qiao, S. Z. Electronic and Structural Engineering of Carbon-Based Metal-Free Electrocatalysts for Water Splitting. *Adv. Mater.* **2019**, *31* (13), 1803625.

(12) Song, H. Q.; Li, Y. H.; Shang, L.; Tang, Z. Y.; Zhang, T. R.; Lu, S. Y. Designed controllable nitrogen-doped carbon-dots-loaded MoP nanoparticles for boosting hydrogen evolution reaction in alkaline medium. *Nano Energy* **2020**, *72*, 104730.

(13) Wan, X. K.; Wu, H. B.; Guan, B. Y.; Luan, D. Y.; Lou, X. W. Confining Sub-Nanometer Pt Clusters in Hollow Mesoporous Carbon Spheres for Boosting Hydrogen Evolution Activity. *Adv. Mater.* **2020**, *32* (7), 1901349.

(14) Ahsan, M. A.; Puente Santiago, A. R.; Hong, Y.; Zhang, N.; Cano, M.; Rodriguez-Castellon, E.; Echegoyen, L.; Sreenivasan, S. T.; Noveron, J. C. Tuning of Trifunctional NiCu Bimetallic Nanoparticles Confined in a Porous Carbon Network with Surface Composition and Local Structural Distortions for the Electrocatalytic Oxygen Reduction, Oxygen and Hydrogen Evolution Reactions. *J. Am. Chem. Soc.* **2020**, *142* (34), 14688−14701.

(15) Puente Santiago, A. R.; Fernandez-Delgado, O.; Gomez, A.; Ahsan, M. A.; Echegoyen, L. Fullerenes as Key Components for Low-Dimensional (Photo)electrocatalytic Nanohybrid Materials. *Angew. Chem., Int. Ed.* **2020**, *60*, 122−141.

(16) Puente Santiago, A. R.; He, T.; Eraso, O.; Ahsan, M. A.; Nair, A. N.; Chava, V. S. N.; Zheng, T.; Pilla, S.; Fernandez-Delgado, O.; Du, A.; et al. Tailoring the Interfacial Interactions of van der Waals 1T-MoS_2/C_{60} Heterostructures for High-Performance Hydrogen Evolution Reaction Electrocatalysis. *J. Am. Chem. Soc.* **2020**, *142*, 17923−17927.

(17) Kulkarni, A.; Siahrostami, S.; Patel, A.; Norskov, J. K. Understanding Catalytic Activity Trends in the Oxygen Reduction Reaction. *Chem. Rev.* **2018**, *118* (5), 2302−2312.

(18) Liu, D. B.; Li, X. Y.; Chen, S. M.; Yan, H.; Wang, C. D.; Wu, C. Q.; Haleem, Y. A.; Duan, S.; Lu, J. L.; Ge, B. H.; et al. Atomically dispersed platinum supported on curved carbon supports for efficient electrocatalytic hydrogen evolution. *Nat. Energy* **2019**, *4* (6), 512−518.

(19) Tahini, H. A.; Tan, X.; Smith, S. C. Unraveling the Factors Behind the Efficiency of Hydrogen Evolution in Endohedrally Doped C-60 Structures via Ab Initio Calculations and Insights from Machine Learning Models. *Adv. Theory Simul.* **2019**, *2* (3), 1800202.

(20) He, T. W.; Gao, G. P.; Kou, L. Z.; Will, G.; Du, A. J. Endohedral metallofullerenes (M@C60) as efficient catalysts for highly active hydrogen evolution reaction. *J. Catal.* **2017**, *354*, 231−235.

(21) Yang, S. F.; Kalbac, M.; Popov, A.; Dunsch, L. A facile route to the non-IPR fullerene Sc3N@C-68: Synthesis, spectroscopic characterization, and density functional theory computations (IPR = isolated pentagon rule). *Chem. - Eur. J.* **2006**, *12* (30), 7856−7863.

(22) Chaur, M. N.; Valencia, R.; Rodriguez-Fortea, A.; Poblet, J. M.; Echegoyen, L. Trimetallic Nitride Endohedral Fullerenes: Experimental and Theoretical Evidence for the M_3N^{6+}@$C_{-2n}^{(6-)}$ model. *Angew. Chem., Int. Ed.* **2009**, *48* (8), 1425−1428.

(23) Solomon, G.; Mazzaro, R.; You, S. J.; Natile, M. M.; Morandi, V.; Concina, I.; Vomiero, A. Ag_2S/MoS_2 Nanocomposites Anchored on Reduced Graphene Oxide: Fast Interfacial Charge Transfer for Hydrogen Evolution Reaction. *ACS Appl. Mater. Interfaces* **2019**, *11* (25), 22380−22389.

(24) Zhang, Y.; Shi, M. T.; Wang, C. Z.; Zhu, Y. X.; Li, N. W.; Pu, X.; Yu, A. F.; Zhai, J. Y. Vertically aligned NiS_2/CoS_2/MoS_2 nanosheet array as an efficient and low-cost electrocatalyst for hydrogen evolution reaction in alkaline media. *Science Bull.* **2020**, *65* (5), 359−366.

(25) Cui, Y.; Zhang, R.; Zhang, J.; Wang, Z. K.; Xue, H. T.; Mao, W. W.; Huang, W. Highly active and stable electrocatalytic hydrogen evolution catalyzed by nickel, iron doped cobalt disulfide@reduced graphene oxide nanohybrid electrocatalysts. *Mater.Today Energy* **2018**, *7*, 44−50.

(26) Zhang, J.; Cui, R. J.; Li, X. A.; Liu, X. H.; Huang, W. A nanohybrid consisting of NiPS3 nanoparticles coupled with defective graphene as a pH-universal electrocatalyst for efficient hydrogen evolution. *J. Mater. Chem. A* **2017**, *5* (45), 23536−23542.

(27) Huang, Z. D.; Liu, J. H.; Xiao, Z. Y.; Fu, H.; Fan, W. D.; Xu, B.; Dong, B.; Liu, D.; Dai, F. N.; Sun, D. F. A MOF-derived coral-like NiSe@NC nanohybrid: an efficient electrocatalyst for the hydrogen evolution reaction at all pH values. *Nanoscale* **2018**, *10* (48), 22758−22765.

(28) Shan, J. Q.; Zheng, Y.; Shi, B. Y.; Davey, K.; Qiao, S. Z. Regulating Electrocatalysts via Surface and Interface Engineering for Acidic Water Electrooxidation. *ACS Energy Lett.* **2019**, *4* (11), 2719−2730.

(29) Valencia, R.; Rodriguez-Fortea, A.; Clotet, A.; de Graaf, C.; Chaur, M. N.; Echegoyen, L.; Poblet, J. M. Electronic Structure and Redox Properties of Metal Nitride Endohedral Fullerenes M_3N@C_{-2n} (M = Sc, Y, La, and Gd; 2n = 80, 84, 88, 92, 96). *Chem. - Eur. J.* **2009**, *15* (41), 10997−11009.

https://doi.org/10.1021/jacs.0c13002
J. Am. Chem. Soc. 2021, 143, 6037−6042

(30) Lopez, X.; Carbo, J. J.; Bo, C.; Poblet, J. M. Structure, properties and reactivity of polyoxometalates: a theoretical perspective. *Chem. Soc. Rev.* **2012**, *41* (22), 7537−7571.
(31) Soriano-Lopez, J.; Musaev, D. G.; Hill, C. L.; Galan-Mascaros, J. R.; Carbo, J. J.; Poblet, J. M. Tetracobalt-polyoxometalate catalysts for water oxidation: Key mechanistic details. *J. Catal.* **2017**, *350*, 56−63.
(32) Campanera, J. M.; Bo, C.; Poblet, J. M. General rule for the stabilization of fullerene cages encapsulating trimetallic nitride templates. *Angew. Chem., Int. Ed.* **2005**, *44*, 7230−7233.
(33) Nørskov, J. K.; Bligaard, T.; Logadottir, A.; Kitchin, J. R.; Chen, J. G.; Pandelov, S.; Stimming, U. Trends in the exchange current for hydrogen evolution. *J. Electrochem. Soc.* **2005**, *152* (3), J23−J26.
(34) Seh, Z. W.; Kibsgaard, J.; Dickens, C. F.; Chorkendorff, I. B.; Norskov, J. K.; Jaramillo, T. F. Combining theory and experiment in electrocatalysis: Insights into materials design. *Science* **2017**, *355*, eaad4998.

NOTE ADDED AFTER ASAP PUBLICATION

Due to a production error, the version of this paper that was published ASAP April 6, 2021, contained an error in the title. The revised version was reposted April 8, 2021.

https://doi.org/10.1021/jacs.0c13002
J. Am. Chem. Soc. 2021, 143, 6037−6042